Virtual Dynamic Grid Impedance and Its Impacts on Harmonics and Stability of Inverter Based Resources Plant

Himadry Shekhar das, Student Member, IEEE, Shuhui Li, Senior Member, IEEE, Bing Lu, and Jing Wang

Abstract — Nowadays, a large number of inverter-based resources (IBRs) are integrated into the grid at a single connection point as an IBR plant. In this paper, a virtual dynamic grid impedance concept is introduced to evaluate the harmonics and stability for grid integration of an IBR plant containing multiple IBRs. First, a detailed theoretical study is conducted to build a foundation of the virtual grid impedance concept, which is a dynamic impedance that changes with the number of IBRs added into an IBR plant. Then, based on the new virtual dynamic grid impedance concept, frequency spectrum analysis is performed to explore harmonic impact at the interconnection point for an IBR plant with IBRs having L, LC, and LCL filters, respectively. An electromagnetic transient (EMT) simulation model of a gridconnected IBR plant is developed to explore the harmonics and stability of the IBR plant connected to the grid as well as the reliable operation of IBRs within the plant from the novel virtual equivalent dynamic grid impedance point of view. Hardware experiments are conducted to validate the EMT simulation evaluation. The results show that the number of IBRs added into an IBR plant influences the grid impedance, i.e., grid strength, and the grid impedance variation has multiple impacts on the IBR plant and IBRs within the plant depending on the grid-connected filters of the IBRs.

Index Terms — inverter-based resources, vector control, grid impedance, grid-connected filters, harmonics, stability, weak grid

I. INTRODUCTION

THE modern electric power grid is going through rapid changes due to the introduction of different renewable energy-based sources, such as solar photovoltaic (PV) and wind power plants. Typically, they are connected to the grid through inverters as well as grid-connected filters associated with the inverters and thus called inverter-based resources (IBRs) [1]. The three most common filtering topologies are L, LC, and LCL filters. Each filter type has its own advantages and shortcomings [2].

In most of the cases for PV and wind farms, IBRs are set up in multiple numbers, possibly in hundreds to generate a larger amount of power, which is called an IBR plant [3]. In this setup, the IBRs are joined together via a collector system, and then the cumulative power is transferred to the grid via a transmission line. When hundreds of IBRs operate in the plant structure, the operation becomes even more complicated, and their impact

can vary as the current supplied by the IBRs within the IBR plant increases or decreases [4].

A. Problem description and literature review

The dynamic nature of the grid impedance influences the individual IBR operating performance and can lead to increased harmonic and stability issues in the power system and abnormal operations of IBRs within a plant. A number of incidents have been reported, where undesired harmonics, inter-harmonics, or resonances caused disruption to the power supply [5-9]. Several works of literature investigated the cause and impact of harmonics on IBR power plants [10-12], where they found that either the passive elements in the system and IBR plant [13], or the dynamic impedance induced by power converter controllers may affect the harmonics [14]. The impacts of harmonics include instability problems due to low frequency [15] and high-frequency oscillations [11], and poor power quality injection to the grid [16]. To identify the reasons for harmonics and instability, grid impedance based analysis is a key approach [17], where the concept of short circuit ratio (SCR) at the point of common coupling (PCC) is applied. But, this approach is implemented on small scale, and only a specific filter type (LCL) [18] with or without the consideration of a transmission line [19, 20].

B. Understand dynamic grid impedance

On April 22, 2022, a new IEEE standard, IEEE Std 2800-2022 [21], was published. Unlike IEEE Std 1547 which focuses primarily on individual IBRs [22], IEEE Std 2800 focuses mainly on IBR plants. The main reason for developing the new standard is that there is a significant difference between individual IBR and IBRs in a plant structure. For a large-scale IBR plant which includes hundreds of IBRs, grid-connected filters, transformers, collector lines, etc., the SCR concept should be replaced by composite SCR (CSCR). To investigate the influence of harmonics and stability on the system, a dynamic IBR plant model as well as related theories is necessary. In this paper, such a model is developed and a detailed theoretical analysis of grid interaction with the IBR plant is presented. In particular, this paper introduces a novel concept of virtual equivalent dynamic grid impedance that is affected by the number of IBRs connected online within an IBR

This work is supported by National Science Foundation PFI-RP under grant number 2141067.

H.S. Das and S. Li are with the Department of Electrical & Computer Engineering, The University of Alabama, Tuscaloosa, AL 35487 USA (e-mails: hdas@crimson.ua.edu, sli@eng.ua.edu).

B. Lu is with Sinoma Overseas Development Co., LTD, China (email: lubingark@126.com)

J. Wang is with the National Renewable Energy Laboratory, Golden, CO 80401 USA (e-mails: jing.wang@nrel.gov).

plant to investigate harmonics and stability for the IBR and grid integration. The virtual equivalent grid impedance varies as the number of IBRs added to the plant changes, and its impact on the grid is analyzed from the perspectives of the IBR control mechanism, filter design, and IBR numbers in the plant, all of which could affect the harmonics and resonances of the grid as well as IBR stability within an IBR plant. The virtual impedance study presented in this paper would reveal unique characteristics associated with an IBR plant.

Overall, the special contributions of the paper include: 1) developing a theoretical foundation for a virtual equivalent dynamic grid impedance concept that depends on the number of IBRs connected to the grid, 2) performing a comprehensive harmonic distortion study based on the virtual grid impedance to provide insights on harmonics and stability of IBRs within an IBR plant, 3) carrying out EMT simulation to study the transient performance of an IBR plant containing IBRs equipped with L, LC, and LCL filters, respectively, 4) performing hardware experiment to validate the proposed study and further consolidate the findings on virtual grid impedance impact, and 5) shedding light on the stability of IBR plants based on the virtual dynamic grid impedance concept and evaluate the application of using this concept for IBR plant design and development.

C. Effect and applications of the proposed study

The virtual grid impedance nature presented in this paper has not been reported in the literature and realized and/or accepted by professionals in the IBR industry. Presently, many electric utility companies are facing deteriorated harmonic problems as more IBRs are connected to the distribution or transmission grid in a plant structure [23]. Without the proposed study, the industry still does not know what the cause is for the problems and what direction to investigate to get solutions for these problems. Researchers at NREL have also got similar findings many times during the hardware-in-the-loop (HIL) experiments and field trials [24]. Traditionally, the virtual grid impedance characteristics as reported in this paper were not addressed and considered in the development of an IBR system and/or IBR controller. The study of this paper indicates that the virtual grid impedance concept and model should be considered in developing IBRs and IBR controllers for a plant configuration. This will be increasingly important as more and more IBR and hybrid IBR plants are rapidly emerging.

The organization of the paper is as follows. The characteristics of IBRs as an individual unit and as a plant and the control structure of both are presented in Section II. Section III develops a novel concept of virtual equivalent dynamic grid impedance of an IBR plant. The impacts of virtual equivalent dynamic grid impedance on the harmonic spectrum from both the plant and IBR view points are studied in Section IV. An EMT simulation model is built and a comprehensive EMT simulation analysis is given in Section V about harmonics, resonances, and stability as the number of IBRs connected to the plant increases for IBRs with different filtering schemes. Section VI gives hardware experiment results. Finally, the paper concludes with summary remarks in Section VII.

II. INVERTER-BASED RESOURCES AND IBR PLANT

A. Inverter-based resources

The IBR family includes a doubly-fed induction generator wind turbine (WT) (Type 3), permanent magnet synchronous generator WT (Type 4), solar PV generator, and battery energy storage [25]. Except for the Type 3 WT, others are usually interconnected to the power grid via a full-scale dc/ac inverter as shown in Fig. 1, which is the focus of this paper. For a solar PV generator and Type-4 WT, the active power is unidirectional from an IBR to the grid, but for a battery energy storage, the active power is bidirectional. For all, the reactive power is bidirectional. When a large number of IBRs are connected together, an IBR plant can be formulated to provide power to the electric power grid.

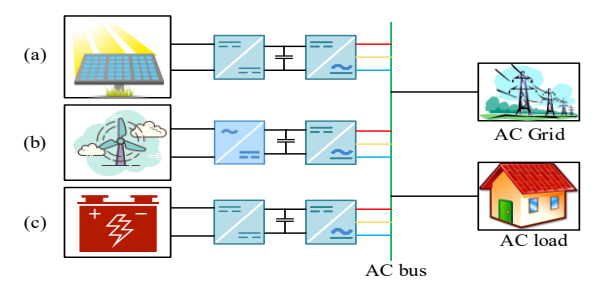


Fig. 1 IBRs with a full-scale dc/ac inverter: a) Solar PV generator, b) Type 4 wind turbine, c) Battery energy storage

B. An IBR Plant

An IBR plant is a group of IBRs in the same location connected together to produce electricity. Typical IBR plants include solar PV plants and wind power plants (WPP). As the cost of solar and wind electricity has continued to fall, the number of grid-connected wind and solar PV plants has grown rapidly. Utility-scale solar PV plants and WPP with hundreds of megawatts have been built worldwide. A WPP can comprise of hundreds to thousands of MW-scale WTs interconnected through a medium-voltage (MV) collector system (typically 34.5 kV), a step-up electrical substation (e.g. 34.5kV/120kV) connected at the POM (point of measurement) to a subtransmission system, a transmission line up to hundred miles, and an interconnection substation that is connected to a much larger bulk power system (BPS) at the POI (point of interconnection). The output terminal of each WT generator is generally 690V and is connected by a step-up transformer to the MV collector system. Fig. 2 presents a generalized gridconnected onshore WPP layout.

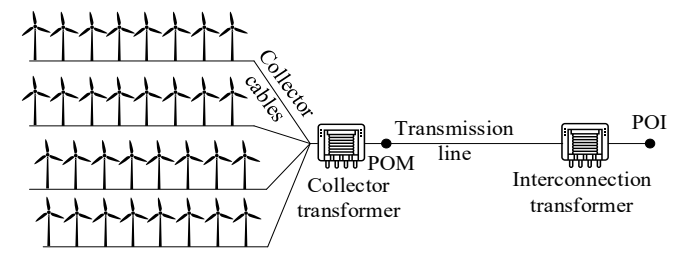


Fig. 2 A generalized grid connected WPP layout

Similarly, large solar power plants have been developed around the globe too. A typical string-inverter-based solar PV

plant consists of hundreds or thousands of strings of PV panels with each string is connected to the collector system via a string-inverter that is equivalent to a WT shown in Fig. 2. Likewise, all the PV strings are connected to a step-up collector transformer and then interconnected to the transmission grid at the POI through the transmission line and another step-up interconnection transformer.

C. Control of a full inverter interfaced IBR and IBR Plant

As shown in Fig. 1, a full-inverter interfaced IBR has a common configuration consisting of an IBR-side converter, a dc-link capacitor, and a grid-side converter. The IBR-side converter is generally an ac/dc converter for a Type-4 WT and a dc/dc converter for solar and battery; the grid-side converter is a dc/ac inverter. The task of the controller applied to the IBR-side converter is for power capture from wind/solar or for battery energy management; the task of the controller applied to the grid-side inverter is to maintain a constant dc-link voltage and regulate reactive power to the grid. For an IBR as a whole to the IBR plant, it is equivalent to assume that the dc-link voltage is constant while the controller of the grid-side inverter has a cascaded inner-loop current controller plus an outer-loop active/reactive power controller, usually designed in the dq reference frame as shown in Fig. 3.

The reference power commands to the outer-loop controller of an IBR are typically generated by a plant-level control system according to the grid requirement at the POI or POM (Fig. 3). The outer-loop controller generates d/q-axis reference currents that are presented to the inner-loop current controller, and the current controller generates d/q-axis control voltages, $v^*_{d_inv}$ and $v^*_{q_inv}$. The voltage injected to the grid at the inverter terminal v_{dq_inv} is related to the control voltage as follows [22],

$$v_{dq_inv} = k_{PWM} \cdot v_{dq_inv}^* \tag{1}$$

where k_{PWM} represents the ratio of the IBR terminal voltage to the controller output voltage resulted from the pulse width modulation (PWM) [26]. The purpose of the outer-loop power controller is to adjust the IBR output active and reactive powers at the point of common coupling (PCC) to follow the reference active and reactive power commands, P^*_{PCC} and Q^*_{PCC} from the plant-level controller, at the steady state.

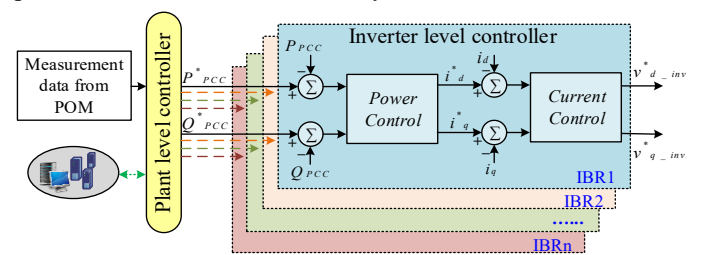


Fig. 3. Control of full inverter interfaced IBRs: plant level control and IBR inverter level control

III. EQUIVALENT CIRCUIT AND DYNAMIC GRID IMPEDANCE OF GRID CONNECTED IBR PLANT

To reduce the harmonic impact, an IBR must be connected to the collector system via a grid filter. The three typical grid filters are L, LC, and LCL filters. Fig. 4 shows the schematic of an IBR with an LCL-filter, in which R_{fl} and L_{fl} are the resistance

and inductance of the inverter-side inductor, C stands for the capacitance of the filter capacitor, R_{fG} and L_{fG} are the resistance and inductance of the grid-side inductor, and R_g and L_g denote the equivalent resistance and inductance looking into the grid at the PCC. The LC and L filters can be considered as special cases of the LCL-filter.

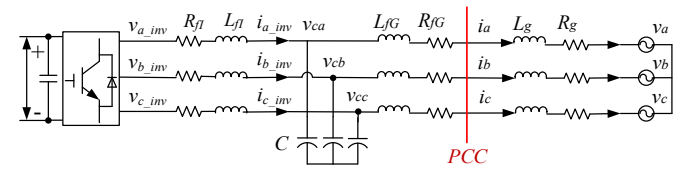


Fig. 4 LCL-filter-based grid-connected converter schematic

In Fig. 4, v_{a,b,c_inv} and v_{d,q_inv} represent the inverter terminal voltage in the 3-phase and dq-reference frame, respectively. Similarly, $v_{a,b,c_PCC}/v_{d,q_PCC}$ are the PCC voltage; $i_{a,b,c_inv}/i_{d,q_inv}$ are the current flowing through the inverter-side inductor; $i_{a,b,c}/i_{d,q}$ are the current flowing through the grid-side inductor and into the BPS at the PCC; $v_{c_a,b,c}/v_{c_d,q}$ are the capacitor voltage; $v_{a,b,c}/v_{d,q}$ are the grid voltage. Thus, the voltage balance equation across the inverter-side inductor is

$$\left[v_{a,b,c_{-}inv} \right] = R_{inv} \left[i_{a,b,c_{-}inv} \right] + L_{inv} \frac{d}{dt} \left[i_{a,b,c_{-}inv} \right] + \left[v_{C_{-}a,b,c} \right]$$
 (2)

The current equation of the LCL capacitor is

$$\left[i_{a,b,c_inv}\right] = \left[i_{a,b,c}\right] + C\frac{d}{dt}\left[v_{C_a,b,c}\right]$$
(3)

The voltage balance equation across the grid-side inductor is

The voltage balance equation across the grid impedance is

$$\left[v_{a,b,c_PCC}\right] = R_g \left[i_{a,b,c}\right] + L_g \frac{d}{dt} \left[i_{a,b,c}\right] + \left[v_{a,b,c}\right]$$
(5)

For an IBR plant (Fig. 2), the equivalent circuit of the IBRs connected to the grid via the collector system is shown in Fig. 5, which can be categized into the following three cases:

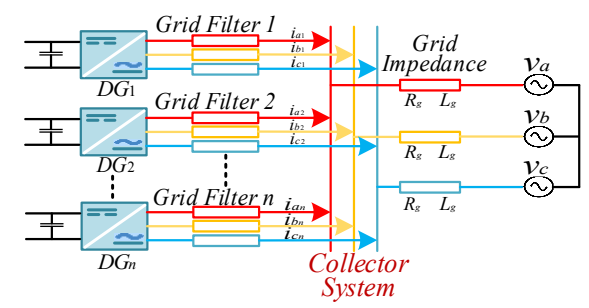


Fig. 5 Schematic of IBRs within an IBR plant connected to the grid

- 1) Neglect the impedance of the collector system. Each IBR within the IBR plant has the same filter parameters and each outputs the same voltage to the AC system at the inverter terminal. For this case, all the inverters are synchronized.
- 2) Neglect the impedance of the collector system. Each IBR within the IBR plant has the same filter parameters and each outputs a different voltage to the three-phase *ac* system at the inverter terminal. For this case, all the inverters are not synchronized and output different voltage and current.

3) Consider the impedance of the collector system. Each IBR within the IBR plant has different filter parameters and each outputs different voltages to the three-phase *ac* system at the inverter terminal.

Let's use superscript k (k=1, 2, ..., N) to distinguish each individual IBR within an IBR plant, where N represents the number of IBRs connected online within an IBR plant. In the following, we will present a theoretical analysis with Case 2 as a representative, in which the voltage at the POM is taken as the reference.

Theorem 1. If each IBR within an IBR plant has the same filter parameters but outputs different voltages to the grid at the inverter terminal, then, from the grid perspective, an IBR plant can be considered as being connected to the grid via a virtually variable filter impedance, that equals to the filter impedance divided by the number of IBRs connected online within an IBR plant, with an output voltage that equals to the average output voltage of all IBRs.

Proof: Since each IBR outputs different voltages but has the same filter parameters, (2) to (5) can be rewritten as

$$\left[v_{a,b,c_inv}^{k}\right] = R_{inv}\left[i_{a,b,c_inv}^{k}\right] + L_{inv}\frac{d}{dt}\left[i_{a,b,c_inv}^{k}\right] + \left[v_{C_a,b,c}^{k}\right]$$
(6)

$$\left[i_{a,b,c_inv}^{k}\right] = \left[i_{a,b,c}^{k}\right] + C\frac{d}{dt}\left[v_{C_a,b,c}^{k}\right] \tag{7}$$

$$\left[v_{C_a,b,c}^k\right] = R_{fG}\left[i_{a,b,c}^k\right] + L_{fG}\frac{d}{dt}\left[i_{a,b,c}^k\right] + \left[v_{a,b,c_PCC}\right]$$
(8)

$$[v_{a,b,c_PCC}] = R_g \sum_{k=1}^{n} [i_{a,b,c}^k] + L_g \frac{d}{dt} \sum_{k=1}^{n} [i_{a,b,c}^k] + [v_{a,b,c}]$$
 (9)

Sum (6), (7), and (8), respectively, for all IBRs, we have

$$\sum_{k=1}^{N} \left[v_{a,b,c_{-}inv}^{k} \right] = R_{inv} \sum_{k=1}^{N} \left[i_{a,b,c_{-}inv}^{k} \right] + L_{inv} \frac{d}{dt} \sum_{k=1}^{N} \left[i_{a,b,c_{-}inv}^{k} \right] + \sum_{k=1}^{N} \left[v_{C_{-}a,b,c}^{k} \right]$$
(10)

$$\sum_{k=1}^{N} \left[i_{a,b,c_inv}^{k} \right] = \sum_{k=1}^{N} \left[i_{a,b,c}^{k} \right] + C \frac{d}{dt} \sum_{k=1}^{N} \left[v_{C_a,b,c}^{k} \right]$$
 (11)

$$\sum_{k=1}^{N} \left[v_{C_{-}a,b,c}^{k} \right] = R_{fG} \sum_{k=1}^{N} \left[i_{a,b,c}^{k} \right] + L_{fG} \frac{d}{dt} \sum_{k=1}^{N} \left[i_{a,b,c}^{k} \right] + N \cdot \left[v_{a,b,c_PCC} \right]$$
(12)

Rewrite (10), (11), (12) and (9) as

$$\sum_{k=1}^{N} \left[v_{a,b,c_inv}^{k} \right] / N = \frac{R_{inv}}{N} \sum_{k=1}^{N} \left[i_{a,b,c_inv}^{k} \right] + \frac{L_{inv}}{N} \frac{d}{dt} \sum_{k=1}^{N} \left[i_{a,b,c_inv}^{k} \right] + \sum_{k=1}^{N} \left[v_{C_a,b,c}^{k} \right] / N$$
(13)

$$\sum_{k=1}^{N} \left[i_{a,b,c_inv}^{k} \right] = \sum_{k=1}^{N} \left[i_{a,b,c}^{k} \right] + \left(N \cdot C \right) \frac{d}{dt} \left(\sum_{k=1}^{N} \left[v_{C_a,b,c}^{k} \right] / N \right)$$
 (14)

$$\frac{1}{N} \sum_{k=1}^{N} \left[v_{C_{-a,b,c}}^{k} \right] = \frac{R_{fG}}{N} \left[i_{a,b,c_{-g}} \right] + \frac{L_{fG}}{N} \frac{d}{dt} \left[i_{a,b,c_{-g}} \right] + \left[v_{a,b,c_{-PCC}} \right]$$
(15)

$$\left[v_{a,b,c_PCC}\right] = R_g \left[i_{a,b,c_g}\right] + L_g \frac{d}{dt} \left[i_{a,b,c_g}\right] + \left[v_{a,b,c}\right]$$
(16)

From (13)-(16), the grid equivalent circuit of an IBR plant with N IBRs is obtained as shown in Fig. 6, which can be considered as an IBR plant being connected to the grid via a virtually

variable grid-filter impedance that is equivalent to the parallel filter impedance of N IBRs connected online within an IBR plant. The IBR plant output voltage v_{a,b,c_inv} is the average of all IBR output voltages and the plant output current is the sum of all the IBR output currents.

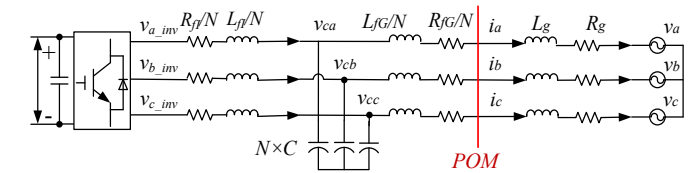


Fig. 6. Grid equivalent circuit of an IBR plant with N LCL-filter-based IBRs

Theorem 2. If each IBR within the IBR plant has the same filter parameters but outputs different voltage to the grid at the inverter terminal, then, from the IBR perspective, it can be considered that an average IBR is connected to the grid via a virtually variable grid impedance that equals to the grid impedance multiplied by the number of IBRs connected online within an IBR plant and the injected voltage of the average IBR is the average of the output voltages of all *N* IBRs.

Proof. Let's rewrite (10), (11), (12) and (9) as

$$\sum_{k=1}^{N} \left[v_{a,b,c_{-}inv}^{k} \right] / N = R_{inv} \sum_{k=1}^{N} \left[i_{a,b,c_{-}inv}^{k} \right] / N + L_{inv} \frac{d}{dt} \sum_{k=1}^{N} \left[i_{a,b,c_{-}inv}^{k} \right] / N + \sum_{k=1}^{N} \left[v_{C_{-}a,b,c}^{k} \right] / N$$
(17)

$$\sum_{k=1}^{N} \left[i_{a,b,c_inv}^{k} \right] / N = \sum_{k=1}^{n} \left[i_{a,b,c}^{k} \right] / N + C \frac{d}{dt} \sum_{k=1}^{N} \left[v_{C_a,b,c}^{k} \right] / N$$
 (18)

$$\frac{\sum_{k=1}^{N} \left[v_{C_{-a,b,c}}^{k} \right]}{N} = R_{fG} \frac{\sum_{k=1}^{n} \left[i_{a,b,c}^{k} \right]}{N} + L_{fG} \frac{d}{dt} \frac{\sum_{k=1}^{n} \left[i_{a,b,c}^{k} \right]}{N} + \left[v_{a,b,c_PCC} \right]$$
(19)

$$[v_{a,b,c_PCC}] = NR_g \frac{\sum_{k=1}^{n} [i_{a,b,c}^k]}{N} + NL_g \frac{d}{dt} \frac{\sum_{k=1}^{n} [i_{a,b,c}^k]}{N} + [v_{a,b,c}]$$
 (20)

From Eqs. (17)-(20), the average equivalent circuit of an IBR within an IBR plant is obtained as shown Fig. 7, in which the average IBR can be considered as being connected to the grid via a variable transmission line impedance that equals to the grid impedance multiplying by the number of IBRs connected online within an IBR plant. The output voltage and current, v_{a,b,c_inv_avg} and i_{a,b,c_inv_avg} , of the average IBR represents the average of the output voltages and currents of all the IBRs.

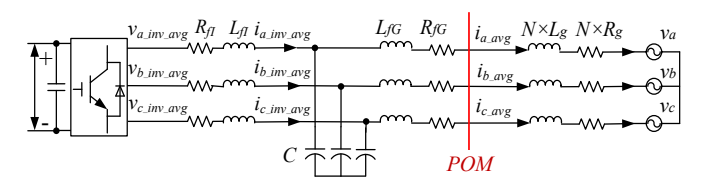


Fig. 7. Equivalent circuit of the LCL-filter-based average IBR within an IBR plant

From Theorems 1 and 2, the following two lemmas can also be obtained for Case 1.

Lemma 1. If each IBR within an IBR plant has the same filter parameters and injects or outputs the same voltage to the grid at

the inverter terminal, then, an IBR can be considered as being connected to the grid via a virtually variable grid impedance that equals to the grid impedance multiplied by the number of IBRs connected online within an IBR plant.

Lemma 2. If each IBR within an IBR plant has the same filter parameters and injects or outputs the same voltage to the grid at the inverter terminal, then, from the grid perspective, an IBR plant can be considered as being connected to the grid via a virtually variable filter impedance that equals to the filter impedance divided by the number of IBRs connected online within an IBR plant.

However, Case 3 is much more complicated than Cases 1 and 2. To develop an analytical IBR plant model for Case 3, either the time domain, such as those shown in (6) to (20), or Laplace transform approach should be utilized. Both will result in very complex state-space system equations, making the developed model extremely difficult to evaluate or simulate. Hence, an approximate model of an IBR plant, based on Theorems 1 and 2 and Lemmas 1 and 2, is proposed for Case 3 as explained below:

1) The IBR within the IBR plant is represented by an average IBR whose output voltage represents the average of the output voltages of all *N* IBRs as follows

$$v_{inv_avg} = \sum_{k=1}^{N} v_{inv}^{k} / N \tag{21}$$

2) The filter parameters of the average IBR are the average of the filter parameters of all IBRs as follows

$$R_{ff_avg} = \sum_{k=1}^{N} R_{ff}^{k} / N, \ L_{ff_avg} = \sum_{k=1}^{N} L_{ff}^{k} / N, \ C_{avg} = \sum_{k=1}^{N} C^{k} / N$$

$$R_{ff_avg} = \sum_{k=1}^{N} R_{fG}^{k} / N, \ L_{ff_avg} = \sum_{k=1}^{N} L_{fG}^{k} / N$$
(22)

3) Regarding the collector system as shown in Fig. 2, assume there are K parallel feeders in the IBR plant and each parallel feeder has N_k series paths. Then, based on the series and parallel natures proved for Cases 1 and 2, the approximate and aggregated average parameters of each feeder of the collector system are obtained as (23a) and the approximate and aggregated average parameters of whole collector system with K parallel feeders are obtained as (23b).

$$R_{k_{-}\text{avg}} = \sum_{i=1}^{N_k} i \cdot R_k^i, \ L_{k_{-}\text{avg}} = \sum_{i=1}^{N_k-1} i \cdot L_k^i$$
 (23a)

$$R_{\text{CS}_\text{avg}} = \sum_{k=1}^{K} R_{k_\text{avg}} / \sum_{k=1}^{K} N_k, \ L_{\text{CS}_\text{avg}} = \sum_{k=1}^{K} L_{k_\text{avg}} / \sum_{k=1}^{K} N_k$$
 (23b)

where R_k^i and L_k^i represent the resistance and inductance of the *i*th series path within the *k*th parallel feeder, and R_{k_avg} and L_{k_avg} represent the approximate and aggregated average resistance and inductance of the *k*th parallel feeder.

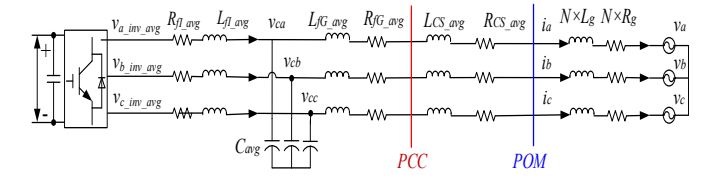


Fig. 8. Equivalent circuit of the LCL-filter-based average IBR within a plant considering different values of IBR filters and collector system impedance

4) With the parameters obtained in (21), (22), and (23), the approximate equivalent circuit model is obtained in Fig. 8.

IV. IMPACTS OF VIRTUAL DYNAMIC GRID IMPEDANCE

An IBR controller is generally developed based on the IBR dynamic equations as shown in (2)-(4) in the d-q reference frame. Usually, the impact of the capacitor (for LCL and LC filters) is omitted when designing the IBR controller [27] so that the dynamic equation of an IBR in the d-q reference frame can be obtained from (2) to (4) as follows:

$$\begin{bmatrix} v_{d_inv} \\ v_{q_inv} \end{bmatrix} = R_f \begin{bmatrix} i_d \\ i_q \end{bmatrix} + L_f \frac{d}{dt} \begin{bmatrix} i_d \\ i_q \end{bmatrix} + \omega_s L_f \begin{bmatrix} -i_q \\ i_d \end{bmatrix} + \begin{bmatrix} v_{d_PCC} \\ v_{q_PCC} \end{bmatrix}$$
(24)

where, $R_f = R_{inv} + R_{fg}$ and $L_f = L_{inv} + L_{fg}$. According to (24) and (4), the grid impact is applied to an IBR at the PCC via the grid impedance $R_g + j \cdot L_g$ in Fig. 6. Basically, the PCC voltage magnitude, distortion, and unbalance can all affect the operation and control of an IBR. The grid impedance is typically determined in terms of the system strength. For an IBR plant, the composite short circuit ratio (CSCR) is used to determine the relative strength of the grid [25]. The CSCR at the POM for an IBR plant is calculated as follows:

$$CSCR_{POM} = SCMVA_{POM} / MW_{IBR-Plant}$$
 (25)

where $SCMVA_{POM}$ is the short circuit MVA level at the POM without the current contribution of the IBR plant, and MW_{IBR_plant} is the total nominal power rating of the IBR plant at the POM. A low $CSCR_{POM}$ ("weak system") indicates a high sensitivity of the POM voltage to changes in power injections at the POM. A high $CSCR_{POM}$ ("stiff") has a low sensitivity of the POM voltage to IBR output.

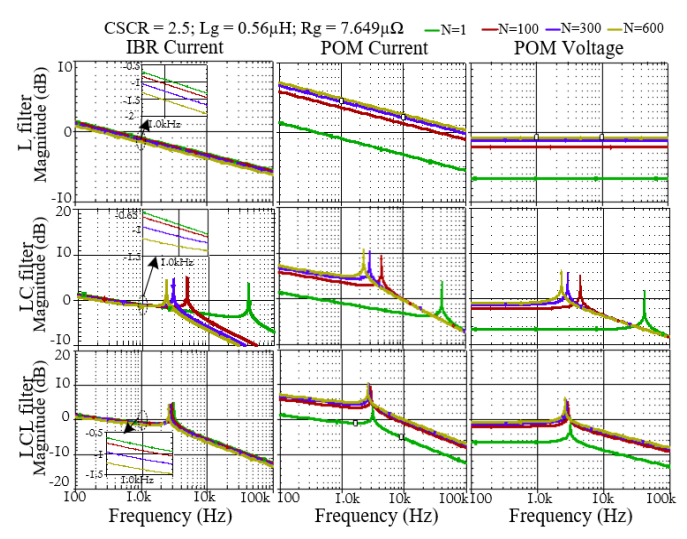
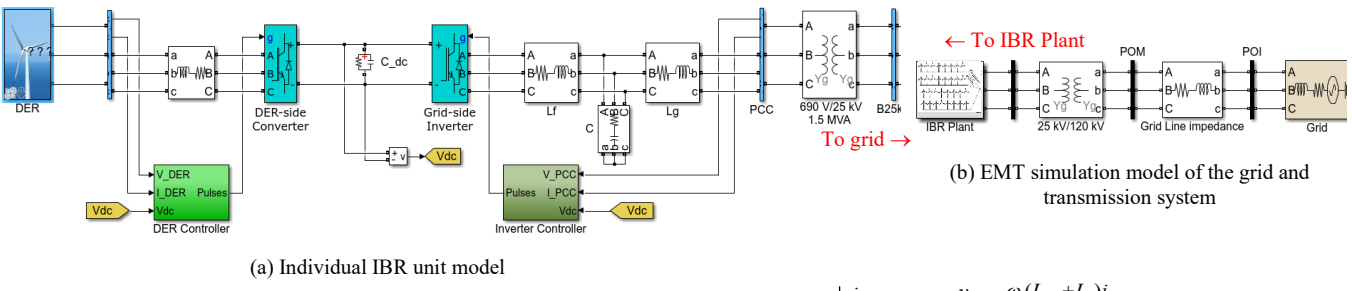


Fig. 9. PCC current and voltage amplitude spectrums

An IBR inverter, as shown in Section II and (1), is typically a voltage source inverter (VSI), meaning that the inverter output a voltage signal to the AC system. Hence, the impact study here is built as follows: 1) The IBR is considered as a voltage source containing fundamental and harmonic components; 2) The IBRs are connected to the grid as an IBR plant as shown in Fig. 2; 3) The system strength is determined



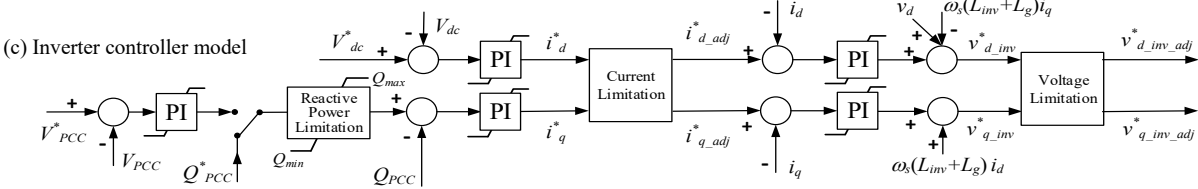


Figure 10. Configuration of individual IBR system within an IBR plant connected to the grid

based on the CSCR discussed above; 4) A new dynamic grid impedance concept, as discussed in Section III, is employed for the impact study; 5) The harmonic spectrum can be done based on either Fig. 6 or Fig. 7. Note: the CSCR is calculated based on the maximum capacity of the IBR plant that is 600 1.5MW IBR units. All three IBR filtering schemes (L, LC and LCL) are considered. The LCL filter has the grid-side and inverter-side inductance of 0.28mH and the capacitance of 55.7 μ F. Detailed design steps of an LCL filter are available in [27] and [28]. For the comparison purpose, we used the same total inductance and capacitance values for the LC and L filters, i.e., the inductance and capacitance values for the LC filter are 0.56mH and 55.7 μ F, respectively, and the inductance value of the L filter is 0.56mH.

PSpice is used for the harmonic spectrum evaluation based on the plant equivalent circuit of Fig. 6 and the average IBR equivalent circuit of Fig. 7, in which the ac sweep simulation is employed to investigate the impact of different harmonic voltages and currents at the POM and how they are affected by IBR injected harmonic voltages and virtually dynamic grid impedance. In terms of Fig. 6, the current spectrum represents the total harmonic current spectrum of all the IBRs within the plant while in terms of Fig. 7, the current spectrum represents the average inverter harmonic current spectrum. Note: the same POM harmonic voltage spectrum can be obtained from either Fig. 6 or Fig. 7. Fig. 9 shows the results of the harmonic spectrums of inverter current, plant current at the POM, and the POM voltage corresponding to a CSCR value of 2.5 (moderate grid) as the number of the IBRs connected to the grid is 1, 100, 300 and 600, respectively. From the figure as well as other results, the following remarks are obtained:

- 1) As the number of the IBRs connected online increases, the POM voltage impact becomes more evident.
- 2) For an IBR with an L filter, the POM voltage increases evenly at high order harmonics as the number of IBRs increases. It is also needed to point out that IBR higher order harmonic contents are typically small though.
- 3) For an IBR with an LC or LCL filter, the impact becomes critical around the resonant frequencies that could be near the IBR current controller crossover frequency and thus affect the IBR control stability.

- 4) The POM voltage stability and harmonics depend not only the system strength but also are affected by the number of IBRs connected to the grid or the virtually grid impedance.
- 5) As the number of IBRs increases, the plant harmonic current spectrum at the POM increases while the inverter harmonic current spectrum decreases a little.
- 6) According to [29, 30], an IBR with a LCL or LC filter can only tolerate the grid impedance variation within 10%. But the study indicates that from the standpoint of multiple IBRs connected to the grid via a transmission line, the virtually grid impedance could shift far beyond the toleration range and thus affect the operation of the IBRs if this is not considered in the IBR design.

V. VIRTUAL GRID IMPEDANCE IMPACT ON HARMONICS AND STABILITY OF IBR PLANT VIA EMT SIMULATION

To evaluate the transient impact of the virtually equivalent dynamic grid impedance on the harmonics and stability of an IBR plant, an EMT simulation of a grid-connected IBR plant was implemented by using MATLAB as shown in Fig. 10, in which each IBR unit is connected to a 690V/25kV step-up transformer via an LCL filter, which can be easily modified as an LC or L filter by removing the grid-side inductor L_{fG} and the capacitor C. Each IBR unit consists of a renewable energy source (RES) on the left (such as a wind turbine or PV array) and the RES controller controls the active power extracted from the RES and sent to the grid based on a reference power command P^* , and the inverter controller controls the interconnection of the IBR with the grid. Each IBR unit, after the step-up transformer, is connected to the grid via the collector system and the transmission line. The grid line voltage at the POI is 120kV, which is connected to the IBR plant (with up to hundreds of IBR units) via an RL element representing the transmission line and a step-down transformer (120kV/25kV) (Fig. 10b).

The detailed configuration of the inverter controller is shown in Fig. 10c, which consists of an inner current controller and an outer *dc*-link voltage controller and a *PCC* voltage or reactive power controller. The conventional dq control frame

[27, 31] was applied to the controller design of each IBR based on the frequency response design technique. The switching frequency of the inverter is 9000Hz and the PCC voltage is fixed at the nominal value. For the current-loop controller, the transfer function is $1/(R_f + s \cdot L_f)$ (Note: the filter capacitor of an LC or LCL filter is typically omitted in the controller design in the literature [27, 31]), the cross-over frequency is 500Hz, and the phase margin is 60 degrees. For the dc-link voltage controller, the transfer function is $\sqrt{3} \cdot m1/(2\sqrt{2} \cdot C \cdot s)$ [32],

the cross-over frequency is 50Hz, and the phase margin is 60 degrees, where m1 is the modulation index and was selected as 0.75 in the design. The designed controller parameters were then tuned for the best performance. The reactive power controller and the PCC bus voltage controller were tuned until a satisfactory performance was achieved.

Before conducting the EMT simulation evaluation of an IBR plant, we first evaluated and compared the aggregated (Fig. 10) and detailed IBR plant models. In general, it was found that if all the IBRs are connected to the POM in parallel, both the aggregated and detailed models basically have the same performance at the POM, which is consistent with the proof shown in Section III for Case 2 condition; if the IBRs are connected to the POM in a series and parallel combination as shown in Fig. 2, the detailed and approximate aggregated plant models are close. Overall, the comparison study shows that the aggregated model (Fig. 10) is effective in evaluating the impact of the virtual grid impedance as presented below for an IBR plant with L, LC, and LCL filters.

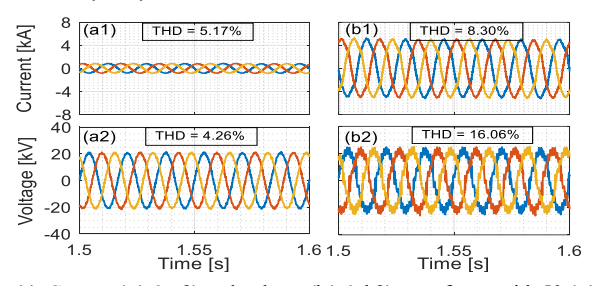


Fig. 11. Current (a1 & a2) and voltage (b1 & b2) waveforms with 50 (a1 & b1) and 300 (a2 & b2) IBR units at a strong (CSCR=4.5) grid condition

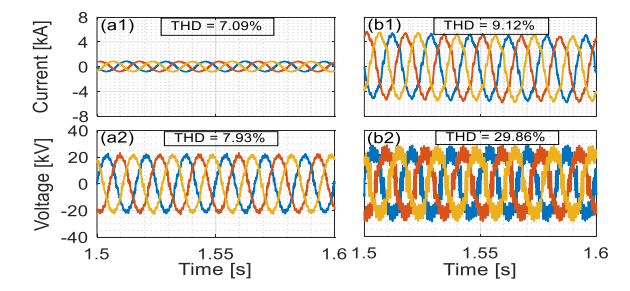


Fig. 12. Current (a1 & a2) and voltage (b1 & b2) waveforms with 50 (a1 & b1) and 300 (a2 & b2) IBR units at a weak (CSCR=1.5) grid condition

A. IBR plant with L-filter IBRs

In this study, all the IBRs within an IBR plant use an L-filter connected to the grid with the number of IBR units within the plant changing from 1 to 600. Fig. 11 shows the current and voltage waveforms at the 25kV bus of the IBR plant corresponding to a strong grid case when each IBR delivers 500 kW active power and 20 kVAR reactive power to the grid. Fig.

12 shows the results at the same power level corresponding to a weak grid case. From the figures and other results, the following remarks are obtained. 1) As the number of the IBRs increases in the plant, more harmonic distortions are found in both the current and voltage waveforms. 2) The impact on the current distortion is less than that on the voltage distortion because the IBR current controller and its filter tries to maintain the current waveform as sinusoidal as possible. 3) The harmonic stability is worse in the weak grid condition especially for the voltage waveform, which could affect the stability of the controller because of the PLL and voltage dq transformation that are needed for the IBR controller.

B. IBR plant with LC-filter IBRs

In this case, all the IBRs within the IBR plant have an LC filter. Figs. 13 and 14 show the current and voltage waveforms at the 25kV bus of the IBR plant corresponding to the strong and weak grid cases, respectively. The power level is the same as those used in Figs. 11 and 12. Compared to the results of the L-filter IBR plant, the current and voltage harmonic distortions are lower under the same number of the IBRs within the IBR plant. This is benefitted by the fact that an LC filter is the second-order filter, which exhibits better damping behaviors than an L filter [33]. However, as the IBR number increases, the resonance of the LC filter causes a significant impact on the stability of the PCC voltage. Especially, as the capacitor is directly connected in parallel to the grid, the resonance would cause a high spike in the PCC voltage (Fig. 13-b2). This situation is even worse for the weak grid case (Fig. 14b) and could cause the IBR controller failure. In the EMT simulation study, we could only get a stable result up to 106 IBRs for the strong grid case and 46 IBRs for the weak grid case.

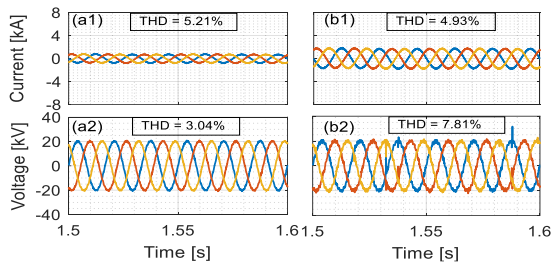


Fig. 13. Current (a1 & a2) and voltage (b1 & b2) waveforms with 46 (a1 & b1) and 106 (a2 & b2) IBR units at a strong (CSCR=4.5) grid condition

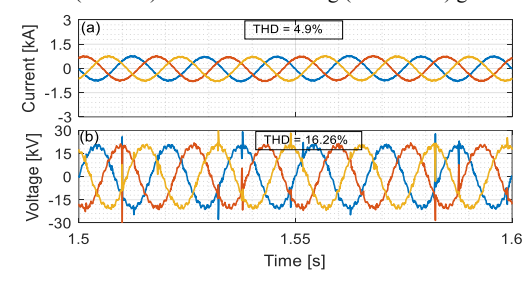


Fig. 14. Current and voltage waveforms at the 25kV bus of the IBR plant with 46 IBR units at a weak (CSCR=1.5) grid condition

C. IBR plant with LCL-filter IBRs

In this case, all the IBRs within the plant have an LCL filter. Figs. 15 and 16 show the results at the strong and weak grid conditions, respectively. Compared to an L- and LC-filter plant, the current and voltage harmonic distortions are lower. This is benefitted by the fact that an LCL filter is a third-order filter,

which exhibits better damping behaviors than an L or LC filter [33]. Compared to the LC-filter plant, the high spike problem of the PCC voltage is resolved as its capacitor is not directly connected to the PCC, which benefits the reliability of the IBR controller. However, as the number of IBRs increases, the resonance impact of the filter dominates the harmonics of the plant and the harmonic distortion deteriorates quickly as the IBRs added to the plant increases. This is more evident in the weak grid condition.

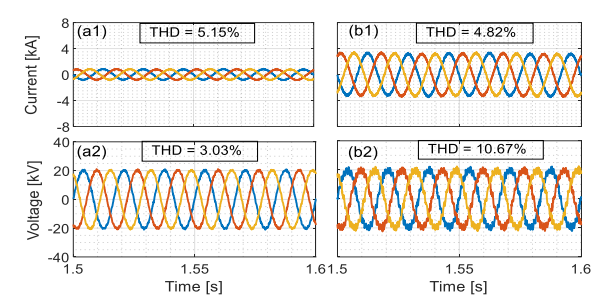


Fig. 15. Current (a1 & a2) and voltage (b1 & b2) waveforms with 50 (a1 & b1) and 200 (a2 & b2) IBR units at a strong (CSCR=4.5) grid condition

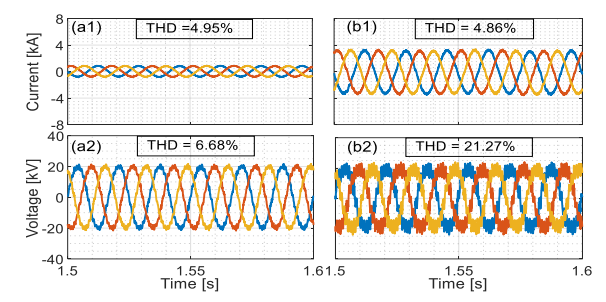


Fig. 16. Current (a1 & a2) and voltage (b1 & b2) waveforms with 50 (a1 & b1) and 200 (a2 & b2) IBR units at a weak (CSCR=1.5) grid condition

D. Summary of an IBR plant with L/LC/LCL-filter IBRs

A more detailed evaluation is given in Table I for the plant containing IBRs with the three different filters at the strong and weak grid conditions, respectively. In general, under the same grid conditions, the L-filter plant can allow more IBRs added into the plant compared to the LCL- or LC-filter plant. The LCL-filter plant has a lower harmonic distortion than the L-filter plant before the resonance starts to dominate as the number of the IBRs added to the plant increases. The LC-filter plant becomes highly unreliable as the number of the IBRs added to the plant increases and is in general not suitable for aggregated interconnection of IBRs to the grid.

From Table I, it is evident that the V-THD increases with the number of IBRs. The reason is that the total harmonics passing through the transmission line (Fig. 2) increase with the IBR number, which causes a higher total harmonic voltage at the PCC as the IBR number increases while the fundamental voltage at the PCC, depending on the grid voltage, is unchanged. Therefore, the V-THD would increase with the number of IBRs connected online.

Different from the V-THD, the I-THD initially decreases slightly and then increases as the number of IBRs increases. The initial drop of the I-THD is consistent with the harmonic current spectrum analysis, shown in Fig. 9 and Section IV, from the inverter perspective. Note: the I-THD is calculated as the total harmonic current RMS over the fundamental current RMS. Thus, the I-THD at the POM for the IBR plant should be

evaluated in comparison with the inverter harmonic current spectrum. However, the spectrum analysis (Fig. 9) does not contain the impact of the harmonic voltages at the POM. As the harmonic voltages at the POM become dominant with a high IBR number, it will affect and increase the inverter I-THD as shown in Table I and Sections IV-A to IV-C as well.

Table I Current and voltage THDs at POM

# of IBRs	Strong grid (CSCR=4.5)						Weak grid (CSCR=1.5)					
	I-THD (%)			V-THD (%)			I-THD (%)			V-THD (%)		
	L	LC	LCL	L	LC	LCL	L	LC	LCL	L	LC	LCL
1	6.28	5.86	5.16	0.59	0.5	0.42	6.26	5.83	5.18	0.84	0.61	0.54
46	6.49	5.21	5.15	4.00	3.04	3.03	7.07	4.9	5.00	7.57	16.26	6.16
50	6.52	5.17	5.15	4.26	3.29	3.19	7.09	N/A	4.95	7.93	N/A	6.68
100	6.87	4.95	4.88	7.08	5.92	5.84	7.91	N/A	4.76	13.05	N/A	12.11
200	7.59	N/A	4.82	11.9	N/A	10.67	9.15	N/A	4.86	21.95	N/A	21.27
300	8.3	N/A	4.65	16.1	N/A	15.16	9.12	N/A	27.2	29.86	N/A	41.95
500	9.29	N/A	5.2	23.1	N/A	22.92		N/A				

Fig. 17 shows the waveforms of the active power, reactive power, and the bus voltage at the POM 25kV side to show the transient response characteristics for an IBR plant with LCL-filter IBRs, in which the active power reference of each IBR in the plant is kept at 500kW, the reactive power reference of each IBR is 100kVAR, and the number of the operating IBRs is initially 0 and changes to 50 from 0.4 to 2 second, 200 from 2 to 4 second, and 400 after 4 second. Note: a rate limiter was applied to each IBR power controller to eliminate the sharp change of the active/reactive power.

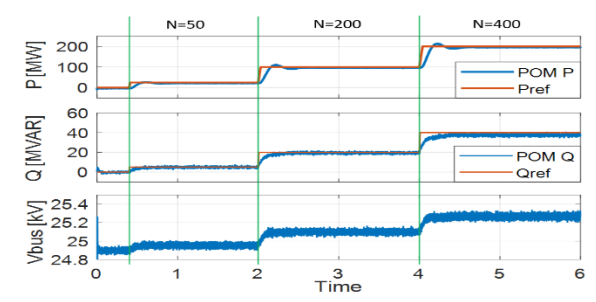


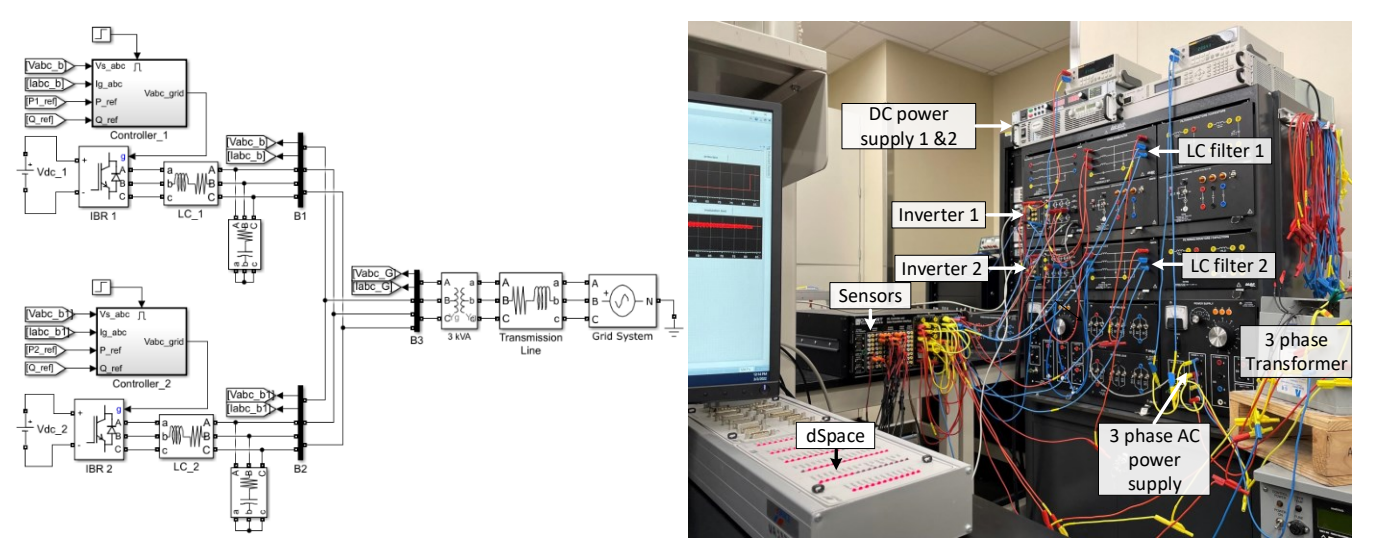
Fig. 17. Active/reactive power and bus voltage at the POM as the number of IBRs (N) changes

E. Further discussion of the case studies

More case studies show that there could be four ways to reduce the impacts of the virtual grid impedance on the stability and THD: 1) increasing the grid strength, 2) adjusting the filter parameters of the IBRs, 3) improving IBR design, and 4) developing new IBR control technologies. Also, other research findings and new approaches could be developed in this field to reduce the impacts in the future.

Firstly, increasing the grid strength would reduce the virtual grid impedance under the same number of IBRs connected online within an IBR plant. This will reduce the PCC voltage THD and thus reduce the THD of the current injected by an IBR into the grid. However, increasing the grid strength could be costly or impractical in some cases.

Secondly, regarding the filter parameters, increasing filter inductance generally reduces the harmonics of the current injected into the grid by an IBR. However, a high inductance value could push an inverter closer to the PWM saturation boundary. Therefore, the design of the filter inductance should consider both the THD and PWM saturation constraint



a) Simulation model of the experiment system

(b)Hardware setup of the experiment system

Fig. 18. Laboratory experiment testing and control systems

requirements for all three types of filters. On the other hand, for LC and LCL filters, reducing the capacitance value of the filters would shift the resonant frequency to a high frequency region [28, 29] and reduce the THD impact caused by the resonance of the filters. However, a too small capacitance value would downgrade an LC or LCL filter to an L filter.

Thirdly, regarding improved IBR system design, this may involve new design strategies for the IBR system by addressing virtual grid impedance impact in the design process.

Fourthly, regarding IBR control technologies, existing IBR control methods, such as the current-loop control, are typically designed based on the transfer function of $1/(R_f + s \cdot L_f)$ without considering the PCC voltage impact. The virtual impedance presented in this paper would make it important to develop new IBR control techniques in the future by considering the PCC voltage impact caused by the virtual grid impedance. In our study, we found that the inverter is affected more by the voltage harmonics at the PCC if the current-loop controller is slow and the inverter is less affected by the voltage harmonics at the PCC if the current-loop controller is fast. However, the design of the controller response speed should also consider the inverter switching frequency and resonant frequency of the LC or LCL filter.

Lastly, among the three filters, the stable operation of an IBR with an LC filter is affected more by the virtual grid impedance. This is due to the fact that the capacitor of an LC filter is directly connected to the PCC. Thus, any PCC voltage disturbance caused by the virtual grid impedance would cause a quick response of the capacitor and affect the stability of the IBR. To reduce the impact, an LCL or L filter would be a better option for IBRs in a plant structure.

Overall, in designing an IBR in a plant structure, the virtual impedance of the grid instead of the grid impedance should be considered in the IBR design process in a plant structure.

VI. HARDWARE EXPERIMENT VALIDATION

To verify the simulation evaluation, a hardware experiment system was built and a series of experiments were conducted.

A. Experimental Setup

The experiment setup is shown in Fig. 18. The IBRs were built by using two LabVolt power converter modules. A three-phase voltage source with a line-line voltage of 208V RMS was utilized to represent the *ac* power grid. The power source was connected to the two inverters via a 3-phase transformer with a turn ratio of $\sqrt{3}/1$. Each inverter had an independent *dc* power supply, was connected to the grid via an LC filter, and was controlled by a separate dSPACE DS1103 system [34]. The two dSPACE control systems were not synchronized.

Each LC filter has L_f =5.7mH, R_f =0.25Ω, C=5μF, and R_C =0.4Ω. The transformer resistance is R_{tr} = 0.4049 and inductance is L_{tr} = 0.483mH. The three-phase ac system approximately has an inductance of L_g =2.4mH and resistance of R_g = 0.0452 (considering X/R = 20). Based on the above parameter values, the CSCR of the experimental two-inverter system is calculated as 3.0439 and the simulation model of the experimental two-inverter system is built as shown in Fig. 18a.

B. Simulation Results

Fig. 19 shows the simulation results of the experimental system. The test sequence is scheduled as follows. Inverter 1 is connected to the grid at t=1 sec and Inverter 2 is connected to the grid at about t=3 sec. The power references of both inverters are 420W and 0VAR, which represents a d-axis current of 3.5A and a q-axis current of 0A. The voltage and current at the transformer output terminal were measured and harmonic levels during the operation of single and two inverters were calculated (Figs. 19a and 19b). The voltage and current THDs were 1.39% and 5.24% when only one inverter was in operation and changed to 1.71% and 3.73% when the second inverter was connected to the grid. This result is consistent with the spectrum analysis shown in Section IV and EMT simulation shown in Section V when the added IBR number is small.

C. Hardware Experimental Results

Fig. 20 shows the experiment results. The test sequence is scheduled as follows, with 0 sec as the starting point for data

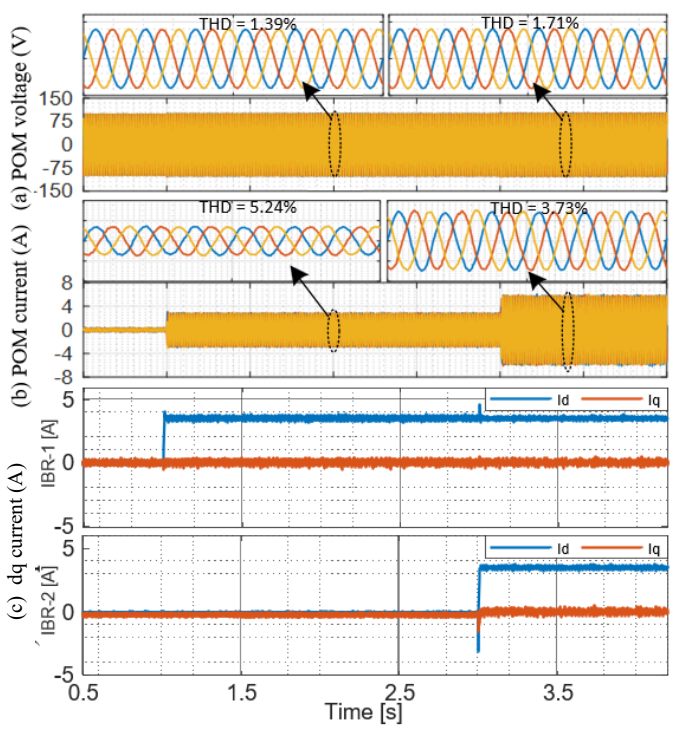


Fig. 19. Simulation results: a) 3-phase POM voltage, b) 3-phase POM current, c) d- and q-axis currents of inverters 1 and 2

recording. Inverter 1 is connected to the grid at t=2 sec and Inverter 2 is connected to the grid at about t=32 sec. The power references of both inverters are 480W and 0VAR, which represents a d-axis current of 4A and a q-axis current of 0A. The voltage and current at the transformer output terminal (POM) were measured and harmonic levels at the POM during the operation of single and two inverters were calculated (Figs. 20a and 20b). In general, the V-THD at the POM was about 3.18% when only one inverter was in operation and changed to 3.86% when two inverters were connected, which is consistent with the voltage harmonic spectrum (Section IV) and EMT simulation (Section V) results. For the I-THD, we found that the I-THD at the POM was about 7.02% when only one inverter was in operation and changed to 5.92% when two inverters were connected, which is consistent with the current harmonic spectrum (Section IV) and EMT simulation (Section V) for low IBR number. However, we also found that the I-THD at the POM was higher sometimes when two inverters were connected, which could be caused by disturbance, noises, and distorted grid voltage that pre-existed in the system. In addition, it was found that when two inverters were connected there were more oscillations in the d- and q-axis currents of the two inverters (Fig. 20c), which was caused by the circulating currents between the two inverters. In general, the experiment results are consistent with the simulation results shown in Fig. 19 and Section V.

VII. CONCLUSIONS

This paper presents a harmonic and stability study of IBR plants based on a new virtually dynamic grid impedance concept developed in the paper. The study shows that the virtual grid impedance varies as the number of IBRs within an IBR plant increases or decreases. This can affect the harmonics and

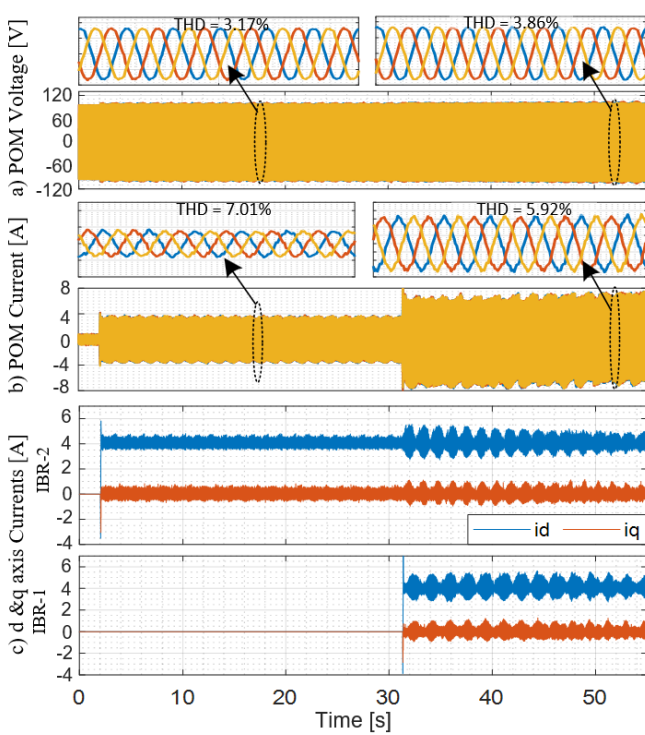


Fig. 20. Experiment results: a) 3-phase POM voltage, b) 3-phase POM current, c) d- and q-axis currents of inverters 1 and 2

stability of the grid and the reliability of the IBR plants too.

The frequency spectrum analysis shows that the change in virtually equivalent grid impedance can heavily impact the operation, harmonics, and stability of an IBR plant. Especially, for an IBR plant with IBRs based upon LC and LCL filters, the resonance effect could magnify the harmonics and instability and significantly deteriorate the reliable operation of IBRs within the plant as the number of IBRs added into an IBR plant increases.

The EMT simulation further demonstrates that under the same grid conditions, the plant with L-filter IBRs can allow a higher equivalent grid impedance value compared to the LCL-filter plant or LC-filter plant. The LCL-filter plant has lower harmonic distortion than the L-filter plant. However, as the virtual grid impedance increases, the resonance impact of the system becomes dominant for an LCL- or LC- filter plant. Especially, an LC-filter plant becomes highly unreliable and is in general not suitable for aggregated interconnection of IBRs to the grid. The simulation study is validated via hardware experiments. Overall, the study shows that the new virtually equivalent dynamic grid impedance impact is an important factor that needs to be considered in the design and development of an IBR plant.

VIII. REFERENCE

- [1] Lu, B., et al. *P-Q Capability Analysis of Inverter Based Resources with Typical Grid Connected Filters.* in *Power and Energy Society General Meeting (PESGM 2020).* 2020. Montreal, Canada: IEEE.
- [2] R. N. Beres, X. Wang, M. Liserre, F. Blaabjerg and C. L. Bak, "A Review of Passive Power Filters for Three-Phase Grid-Connected Voltage-Source Converters," in *IEEE Journal of Emerging and Selected Topics in Power Electronics*, vol. 4, no. 1, pp. 54-69, March 2016, doi: 10.1109/JESTPE.2015.2507203.

- [3] Z. Chen, J. M. Guerrero and F. Blaabjerg, "A Review of the State of the Art of Power Electronics for Wind Turbines," in *IEEE Trans. Power Electronics*, vol. 24, no. 8, pp. 1859-1875, Aug. 2009, doi: 10.1109/TPEL.2009.2017082.
- [4] Luhtala, R., et al., "Identification of Three-Phase Grid Impedance in the Presence of Parallel Converters," Energies, 2019. 12(14): p. 2674.
- [5] Adams, J., C. Carter, and S.-H. Huang. ERCOT experience with subsynchronous control interaction and proposed remediation. in PES T&D 2012. 2012. IEEE.
- [6] C. Hou, M. Zhu, Z. Li, Y. Li and X. Cai, "Inter Harmonic THD Amplification of Voltage Source Converter: Concept and Case Study," in *IEEE Trans. Power Electronics*, vol. 35, no. 12, pp. 12651-12656, Dec. 2020, doi: 10.1109/TPEL.2020.2994751.
- [7] H. Liu et al., "Subsynchronous Interaction Between Direct-Drive PMSG Based Wind Farms and Weak AC Networks," in *IEEE Trans. Power Systems*, vol. 32, no. 6, pp. 4708-4720, Nov. 2017, doi: 10.1109/TPWRS.2017.2682197.
- [8] Li, C., "Unstable operation of photovoltaic inverter from field experiences," IEEE Trans. Power Delivery, 2017. 33(2): p. 1013-1015.
- [9] J. Sun, G. Wang, X. Du and H. Wang, "A Theory for Harmonics Created by Resonance in Converter-Grid Systems," in *IEEE Trans. Power Electronics*, vol. 34, no. 4, pp. 3025-3029, April 2019, doi: 10.1109/TPEL.2018.2869781.
- [10] C. Larose, R. Gagnon, P. Prud'Homme, M. Fecteau and M. Asmine, "Type-III Wind Power Plant Harmonic Emissions: Field Measurements and Aggregation Guidelines for Adequate Representation of Harmonics," in *IEEE Trans. Sustainable Energy*, vol. 4, no. 3, pp. 797-804, July 2013, doi: 10.1109/TSTE.2013.2252209.
- [11] X. Wang and F. Blaabjerg, "Harmonic Stability in Power Electronic-Based Power Systems: Concept, Modeling, and Analysis," in *IEEE Trans. Smart Grid*, vol. 10, no. 3, pp. 2858-2870, May 2019, doi: 10.1109/TSG.2018.2812712.
- [12] Ebrahimzadeh, E., et al., "Harmonic stability and resonance analysis in large PMSG-based wind power plants," *IEEE Trans. Sustainable Energy*, 2017. 9(1): p. 12-23.
- [13] Monjo, L., et al., "Study of resonance in wind parks," Electric Power Systems Research, 2015. 128: p. 30-38.
- [14] Kocewiak, Ł.H., J. Hjerrild, and C.L. Bak, "Wind turbine converter control interaction with complex wind farm systems," *IET Renewable Power Generation*, 2013. 7(4): p. 380-389.
- [15] Bazargan, D., S. Filizadeh, and A.M. Gole, "Stability analysis of converter-connected battery energy storage systems in the grid," *IEEE Trans. Sustainable energy*, 2014. 5(4): p. 1204-1212.
- [16] Ghorbani, M.J. and H. Mokhtari, "Impact of Harmonics on Power Quality and Losses in Power Distribution Systems," *International Journal of Electrical Computer Engineering*, 2015. 5(1).
- [17] Yoon, C., et al., "Harmonic stability assessment for multiparalleled, grid-connected inverters," *IEEE Trans. Sustainable Energy*, 2016. 7(4): p. 1388-1397.
- [18] M. Lu, X. Wang, P. C. Loh and F. Blaabjerg, "Resonance Interaction of Multiparallel Grid-Connected Inverters With LCL Filter," in *IEEE Trans. Power Electronics*, vol. 32, no. 2, pp. 894-899, Feb. 2017, doi: 10.1109/TPEL.2016.2585547.
- [19] X. Wu, X. Li, X. Yuan and Y. Geng, "Grid Harmonics Suppression Scheme for LCL-Type Grid-Connected Inverters Based on Output Admittance Revision," in *IEEE Trans. Sustainable Energy*, vol. 6, no. 2, pp. 411-421, April 2015, doi: 10.1109/TSTE.2014.2384509.
- [20] S. Zhang, S. Jiang, X. Lu, B. Ge and F. Z. Peng, "Resonance Issues and Damping Techniques for Grid-Connected Inverters With Long Transmission Cable," in *IEEE Trans. Power Electronics*, vol. 29, no. 1, pp. 110-120, Jan. 2014, doi: 10.1109/TPEL.2013.2253127.
- [21] "IEEE Standard for Interconnection and Interoperability of Inverter-Based Resources (IBRs) Interconnecting with Associated Transmission Electric Power Systems," in IEEE Std 2800-2022, vol., no., pp.1-180, 22 April 2022, doi: 10.1109/IEEESTD.2022.9762253.
- [22] "IEEE Standard for Interconnection and Interoperability of Distributed Energy Resources with Associated Electric Power Systems Interfaces," in IEEE Std 1547-2018 (Revision of IEEE Std 1547-2003), vol., no., pp.1-138, 6 April 2018, doi: 10.1109/IEEESTD.2018.8332112.
- [23] The National Grid Sugar Hill PV farm, available at https://www.commonenergy.us/projects/sugarhill.
- [24] J. Wang, A. Pratt, K. Prabakar, B. Miller, M. Symko-Davies, "Development of an integrated platform for hardware-in-the-loop evaluation of microgrids prior to site commissioning," *Applied Energy*, vol. 290, May 2021, https://doi.org/10.1016/j.apenergy.2021.116755.

- [25] NERC, Integrating Inverter-Based Resources into Low Short Circuit Strength Systems Reliability Guideline. 2017.
- [26] Mohan, N., Advanced electric drives: analysis, control, and modeling using MATLAB/Simulink. 2014: John wiley & sons.
- [27] M. Liserre, F. Blaabjerg, and S. Hansen, "Design and control of an LCL filter-based three-phase active rectifier," *IEEE Trans. Ind. Appl.*, vol. 41, no. 5, pp. 1281–1291, Oct. 2005.
- [28] S. Jayalath and M. Hanif, "Generalized LCL-Filter Design Algorithm for Grid-Connected Voltage-Source Inverter," in *IEEE Trans. Industrial Electronics*, vol. 64, no. 3, pp. 1905-1915, March 2017, doi: 10.1109/TIE.2016.2619660.
- [29] P. Channegowda and V. John, "Filter Optimization for Grid Interactive Voltage Source Inverters," in *IEEE Trans. Industrial Electronics*, vol. 57, no. 12, pp. 4106-4114, Dec. 2010, doi: 10.1109/TIE.2010.2042421.
- [30] D. Yang, X. Ruan and H. Wu, "Impedance Shaping of the Grid-Connected Inverter with LCL Filter to Improve Its Adaptability to the Weak Grid Condition," in *IEEE Trans. Power Electronics*, vol. 29, no. 11, pp. 5795-5805, Nov. 2014, doi: 10.1109/TPEL.2014.2300235.
- [31] V. Blasko and V. Kaura, "A novel control to actively damp resonance in input LC filter of a three-phase voltage source converter," *IEEE Trans. Ind. Appl.*, vol. 33, no. 2, pp. 542–550, Mar./Apr. 1997.
- [32] R. Pena, J.C. Clare, and G.M. Asher, "Doubly fed induction generator using back-to-back PWM converters and its application to variable-speed wind-energy generation," *IEE Proc. Electr. Power Appl.*, Vol. 143, No 3, May 1996.
- [33] Lettl, J., Bauer, J., and Linhart, L., "Comparison of different filter types for grid connected inverter," Progress in Electromagnetics Research Symposium Proceedings, pp. 1426–1429, Marrakesh, Morocco, 20–23 March 2011.
- [34] A. Thomas, "dSPACE DS1103 Control Workstation Tutorial and DC Motor Speed Control," Senior Project Report, Bradley University ECE Department, May 11, 2009.



Himadry Shekhar Das (S'19) received his M.Phil degree from the School of Electrical Engineering, Universiti Teknologi Malaysia, Johor Bahru, Malaysia in 2018 and B.Sc. from Dept of Electrical and Electronic Engineering, Ahsanullah University of Science and Technology (AUST), Dhaka, Bangladesh in 2010. He is currently a Ph.D. student of the Department of Electrical and

Computer Engineering, The University of Alabama, Tuscaloosa, U.S.A. He is now engaged with research activities related to power electronics, renewable energy, electric vehicles, and grid integration of inverter-based resources. He has published more than twenty journal and conference articles during his journey, also volunteering as a reviewer in several prestigious journals.



Shuhui Li (S'99–M'99–SM'08) received the B.S. and M.S. degrees in electrical engineering from Southwest Jiaotong University, Chengdu, China, in 1983 and 1988, respectively, and the Ph.D. degree in electrical engineering from Texas Tech University, Lubbock, TX, USA, in 1999. He was with the School of Electrical Engineering, Southwest Jiaotong University, from 1988 to 1995, where his fields of research interest included

electrified railways, power electronics, power systems, and power system harmonics. From 1995 to 1999, he was engaged in research on wind power, artificial neural networks, and applications of massive parallel processing. He joined Texas A&M University, Kingsville, TX, USA, as an Assistant Professor, in 1999, and an Associate Professor in 2003. He joined the University of Alabama, Tuscaloosa, AL, USA, as an Associate Professor, in 2006. He is a Voting Member of the IEEE 2800, P2030, 2418.5, and P2030.12 working groups, involving the IEEE standardization works on Interconnection and Interoperability of Inverter-Based Resources, Smart Grid Interoperability, Blockchain in Energy, and Microgrid Protection Systems. His current research interests include renewable energy systems, power electronics, power systems, electric machines and drives, and applications of artificial intelligence and machine learning in power and energy systems.



Bing Lu received the B.S. degree in electrical engineering from The University of Oklahoma, Norman, OK, USA in 2016, M.S. degree in electrical engineering from The University of Alabama, Tuscaloosa, AL, USA in 2021. He is currently working with SINOMA Overseas Development CO., LTD. His major research interests include power systems, power electronics, renewable energy, and converter design and control.



Jing Wang (S'10–M'11–SM'21) received Ph.D. degree in electrical engineer from RWTH Aachen University, Germany, in 2015. Currently, Dr. Jing Wang is a Senior Research Engineer at the National Renewable Energy Laboratory. Her research focuses on power electronics control of distributed energy resources, microgrid modeling, protection design, and control, distributed energy resources (DERs)

integration. She has expertise in power and controller hardware-in-the-loop (HIL) evaluation of microgrid controller, advanced distribution management system (ADMS), distributed energy resource management system (DERMS) and DERs for grid automation and control, and DER integration studies.